Assessing the Potential of Biochars Prepared by Steam-Assisted Slow Pyrolysis for CO 2 Adsorption and Separation

Valentina Gargiulo, Alicia Gomis-Berenguer, Paola Giudicianni, Conchi Maria Concepcion Ovin Ania, Raffaele Ragucci, Michela Alfè

energy&fuels

Article

Cite This: Energy Fuels 2018, 32, 10218−10227

pubs.acs.org/EF

Assessing the Potential of Biochars Prepared by Steam-Assisted Slow Pyrolysis for CO_2 Adsorption and Separation

Valentina Gargiulo,*[,†] Alicia Gomis-Berenguer,[‡] Paola Giudicianni,[†] Conchi O. Ania,[‡] Raffaele Ragucci,[†] and Michela Alfè[†]

[†]Istituto di Ricerche sulla Combustione (IRC), Consiglio Nazionale delle Ricerche (CNR), Piazzale Vincenzo Tecchio 80, 80126 Napoli, Italy

[‡]POR2E Group, CEMHTI CNRS (UPR 3079), Université d'Orléans, 45071 Orléans, France

Supporting Information

ABSTRACT: The potentialities in the use of biochars prepared by steam-assisted slow pyrolysis as adsorbents of gases of strategic interest (N_2, CO_2, and CH_4) and their mixtures were explored. The biochars prepared from *Populus nigra* wood and cellulose fibers exhibited a narrow microporosity, with average pore sizes ranging between 0.55 and 0.6 nm. The micropore volume increased with the pyrolysis temperature, allowing CO_2 and CH_4 uptakes at room temperature between 1.5 and 2.5 mmol/g and between 0.1 and 0.5 mmol/g, respectively. These values are in line with those from the literature on biomass-derived carbon-based materials, exhibiting much higher porous features than those reported herein. As for the separation of CO_2/N_2 and CO_2/CH_4 gas mixtures, data showed that the prepared biochars exhibited good selectivities for CO_2 over both N_2 and CH_4: between ca. 34 and 119 for a CO_2/N_2 mixture in typical post-combustion conditions (15:85, v/v) and between 14 and 34 for a CO_2/CH_4 mixture typical of natural gas upgrading (30:70, v/v).

INTRODUCTION

A biochar is a carbon-based solid product obtained through thermochemical conversions, such as pyrolysis, gasification, torrefaction, and hydrothermal carbonization of biomass.[1,2] The number and type of potential feedstocks for biochar production are huge, e.g., wood and agricultural wastes, rice husks and straw, leaves, food waste, paper sludge, bagasse, and many others.[1,2] Under certain operating conditions, biochar production is an energy self-sufficient process and can produce biofuel for use in various energy conversion processes, including transportation and electricity production.[3] This means that agricultural and animal waste disposal can be reduced by recycling the waste, using pyrolysis, into biochar, energy, and value-added products.

Biochars consist of fixed carbon, ash components, moisture, and, on the basis of production conditions, labile carbon and other volatile compounds.[4−6] These materials have recently attracted much attention as inexpensive, environmentally friendly, carbon-rich materials with potential applications in a variety of fields, such as soil remediation, waste management, greenhouse gas reduction, and energy production.[4−9] New applications using biochar as material for electronics and bioenergy (fuel cells and supercapacitors), as a catalyst for syngas cleaning and conversion of syngas to liquid hydrocarbon, and as a sorbent for contaminant reduction in gaseous streams are emerging.[1,10−13] Because there is a limited literature on the applications of the biochar as a gas adsorbent and/or catalyst, research efforts in this field are of great importance.

On the other hand, adsorption on a solid matrix represents a well-assessed method for the capture and separation of CO_2 from exhaust flue gases.[14,15] An ideal CO_2 adsorbent should (i) exhibit high selectivity toward CO_2 over N_2 and other exhaust components (CO, NH_3, and light hydrocarbons, such as CH_4), (ii) be produced via inexpensive and low-energy consumption processes, using renewable resources as precursors, (iii) exhibit flexible morphologies, pore structures, and functionalities, and (iv) present good mechanical properties to undergo repeated adsorption−desorption cycles.[15,16] In this framework, the biochar is gaining a lot of interest because it could represent a valid low-cost substitute of the more expensive activated carbons.

With these premises, the aim of this work was to assess the potential of biochars prepared from steam-assisted slow pyrolysis of biomass feedstocks (*Populus nigra* wood and cellulose fibers) in carbon capture and storage applications. For this, a series of biochars with different characteristics were prepared by steam-assisted slow pyrolysis and tested to adsorb and separate CO_2 from N_2 and CH_4 in a typical scenario of flue gases. Although slow pyrolysis is typically carried out in an inert atmosphere, the presence of oxidant agents, such as steam, has been reported to improve the porosity of the chars as a result of its ability to efficiently penetrate on the precursor during the slow pyrolysis, enhancing devolatilization, and, if the temperature is high enough, to promote gasification reactions.[17−21] The gas adsorption and selectivity were measured by means of equilibrium adsorption isotherms for pure gases at ambient conditions. In particular, gas adsorption data were used to predict the adsorption of binary mixtures

Special Issue: SMARTCATs COST Action

Received: March 27, 2018
Revised: June 1, 2018
Published: June 8, 2018

DOI: 10.1021/acs.energyfuels.8b01058
Energy Fuels 2018, 32, 10218−10227

and determine CO_2/N_2 and CO_2/CH_4 selectivities by applying the ideal adsorbed solution theory (IAST).

EXPERIMENTAL SECTION

Biochar Precursors. *P. nigra* wood and cellulose fibers were used as biomass feedstocks for the preparation of the biochars. *P. nigra* wood was selected as a precursor because it allows for the production of a biochar with a higher specific surface area compared to other lignocellulosic biomasses treated in the same pyrolytic conditions.[17] Moreover, *P. nigra* is among the faster growing trees for short rotation coppice, with an annual dry matter production of 17.8 Mg ha^{-1} $year^{-1}$.[17] Cellulose fibers were selected as model feedstock; cellulose is one of the three main biomass components, and the most abundant component in *P. nigra* wood (55.4 wt % cellulose, 11.6 wt % lignin, and 26.8 wt % hemicellulose).[17]

Synthesis of the Biochars. Biochars were produced from *P. nigra* wood and cellulose fibers (Sigma-Aldrich C6663) through a steam-assisted slow pyrolysis process as described in previous works.[17,18] Briefly, the biomass (400−600 μm size range) was pre-dried in a thermoventilated oven at 105 °C for 2 h to remove the residual moisture before the pyrolysis experiments. Then, about 6 g of biomass were spread as thin layers (approximately 1 mm thick) over four trays in the pyrolytic reactor[18] and exposed to steam flow (ca. 0.25 g/s, with an average residence time of 2 s) up to the desired temperature (480−700 °C). The heating rate was fixed to ca. 5 °C/min and pressure to ca. 5×10^5 Pa. Gaseous stream driven by the flux of steam exited the reaction unit and passed through a condensation device, and the permanent gases were sent to the exhaust. Biochar was recovered from the trays at the end of each experimental test, and the yield was determined gravimetrically with respect to the fed sample. The reliability of the experimental apparatus has been evaluated on two replicates of the same experimental run, and an absolute error lower than 5% of the measured values has been observed for the yields of solid. Biochars from cellulose fibers were prepared at three pyrolysis temperatures of 530, 650, and 700 °C, and biochars from *P. nigra* wood were obtained at 480 and 600 °C. As reported in previous works,[17,18] these temperatures have been selected on the basis of the thermal degradation profiles of the biochar precursors (Figure S1 of the Supporting Information). Moreover, in accordance with the results reported in previous works, to obtain chars with a well-developed porosity, pyrolysis temperatures below 480 °C were discarded as a result of the incomplete thermal degradation of the biomass precursors.[17,18,22] The nomenclature of the biochars will be CEL-T and PN-T for those obtained from cellulose fibers and *P. nigra* wood precursors, respectively, where T refers to the final temperature of the steam-assisted slow pyrolysis process applied for the production of the sample.

Characterization Methods. The carbon, hydrogen, and nitrogen contents of the samples were measured by a CHN 628 LECO elemental analyzer according to the ASTM E870 procedure using ethylenediaminetetraacetic acid (EDTA) as the standard. For each sample, two replicates were performed and the average values are reported (maximum relative error of around 0.7%). The ash content was evaluated by thermogravimetric analysis in a TGA 701 LECO analyzer. Fourier transform infrared spectroscopy (FTIR) analysis of the biochars was performed on solid sample dispersions prepared by mixing and grinding the powdered materials (0.5−0.8 wt %) with KBr. Pellets of the biochar and KBr mixtures were obtained upon compression at 10 tons for 10 min. FTIR spectra in the 3400−600 cm^{-1} range were acquired in the transmittance mode using a 5700 Nicolet spectrophotometer. Each spectrum was obtained by collecting 32 interferograms with 0.02 cm^{-1} resolution. The porosity of the biochars was characterized by gas adsorption experiments. High-resolution equilibrium nitrogen adsorption/desorption isotherms at −196 °C were collected in a volumetric analyzer (Triflex, Micrometrics) provided with three pressure transducers to allow for high resolution in the low pressure range. The samples were previously outgassed under dynamic vacuum (ca. 10^{-5} Torr) at 120 °C overnight. The Brunauer−Emmett−Teller (BET) theory was used to calculate the specific surface areas and total pore volumes. Additionally, the narrow microporosity was assessed by CO_2 equilibrium adsorption/desorption isotherms at 0 °C (Tristar II 3020, Micrometrics). The micropore volumes were evaluated using the Dubinin−Radushkevich (DR) formulism applied to nitrogen gas adsorption data. The narrow microporosity was further evaluated from the CO_2 adsorption/desorption isotherms at 0 °C, using the DR equation and the two dimensional non-local density functional theory (2D-NLDFT) method.[23] Ultrapure gases were used for all of the measurements. The reproducibility of the adsorption data was assessed by measuring the adsorption isotherms on at least two fresh aliquots of selected samples.

Gas Adsorption Tests. Gas adsorption/desorption isotherms of selected gases (i.e., CO_2, CH_4, and N_2) at temperatures near ambient (i.e., 0, 10, and 25 °C) were collected in a volumetric instrument (Tristar II 3020, Micromeritics) in the pressure range of 0.1−900 Torr. Gas adsorption data near room temperature were recorded with over 60 points in the whole range of relative pressures, with readings at least every ca. 1.5 cm^3/g to obtain accurate data. The analyzer is equipped with a pressure transducer of 1000 mmHg capacity (accuracy within 0.15% of reading). The outgassing conditions before the adsorption measurements were as indicated above. The temperature of the analysis was maintained using a water circulating bath. The CO_2 isosteric heats of adsorption were calculated using the Clausius−Clapeyron equation with the specific tool of Microactive software (Micromeritics) from the set of equilibrium isotherms acquired at near ambient conditions (0, 10, and 25 °C). The isosteric enthalpies of adsorption were obtained from the slopes of the lines in the plots of ln P versus $1/T$ for a given amount adsorbed in the isotherms at different temperatures. An average Q_{st} value was calculated over the whole range of CO_2 uptakes. The IAST was used to predict binary mixture adsorption from the experimental pure gas isotherms.[24] The integration required by IAST was achieved by fitting the single-component gas isotherms to the Jensen equation.[25] Typical conditions of flue gases in post-combustion processes (e.g., CO_2/N_2 mixtures of 15:85, v/v) and natural gas fields (e.g., CO_2/CH_4 mixtures of 30:70, v/v) were used in the binary mixture predictions. Selectivity for gas component i over j (S_{ij}) was calculated at 25 °C and 1 atm as $S_{ij} = C_i/x_j/C_j/x_i$, where C_i and C_j are the modeled adsorbed amounts of components i and j in the mixture and x_i and x_j are their molar fractions in the mixture.

RESULTS AND DISCUSSION

Biochar Compositional Properties. The chemical composition of the synthesized biochars is listed in Table 1.

Table 1. Chemical Composition of the Biochars (Dry and Ash-Free Basis)

	CEL-530	CEL-650	CEL-700	PN-480	PN-600
C (wt %)	85.40	88.40	83.70	80.70	89.60
H (wt %)	2.40	2.20	0.60	3.50	2.60
N (wt %)	0	0	0	0.70	1.00
O (wt %)[a]	12.20	9.40	15.70	15.10	6.80
ash (wt %)	0	0	0	8.70	12.80
H/C	0.34	0.30	0.09	0.52	0.35
O/C	0.11	0.08	0.14	0.14	0.06
yield (wt %)	18	16	16	27	21

[a]Calculated by difference

H/C and O/C atomic ratios are also reported, because they correlate with the degree of aromaticity and polarity of the biochars, respectively.[26] The ash content of the biochars obtained from cellulose fibers was negligible, in agreement with previous results[18] and as opposed to those obtained from *P. nigra* wood feedstock.[17] The biochar yields ranged from 16 to 27 wt %, being higher in the biochars obtained from *P. nigra*

DOI: 10.1021/acs.energyfuels.8b01058
Energy Fuels 2018, 32, 10218−10227

and following the expected decreasing trend with the pyrolysis temperature for a given precursor (Table 1).

With regard to chemical composition, all of the prepared biochars are rich-carbon materials. As a general rule, the carbon content increased with the pyrolysis temperature, with the exception of CEL-700. This is attributed to a higher extent in the devolatilization reactions of the precursor under a steam/nitrogen flow; for the case of CEL-700, the temperature might be too high, leading to the consumption of carbon.[18] The decrease of the H/C values with the pyrolysis temperature indicates the higher aromatic character of the chars obtained at higher temperatures. A similar trend was reported for biochars from other biomass precursors.[17,26] On the other hand, the polarity of the biochars, evaluated on the basis of the O/C values, is quite similar (Table 1).

The analysis of infrared spectra confirmed the presence of an aromatic carbonaceous network in all of the biochars. As seen in Figure 1, all of the samples were characterized by broad-

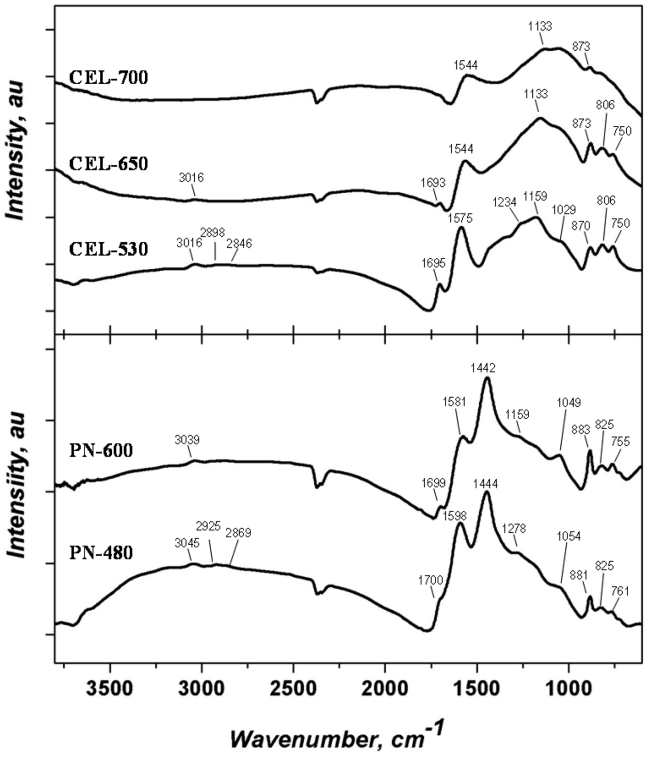

Figure 1. FTIR spectra of biochars synthesized from (top) cellulose fibers and (bottom) *P. nigra* wood.

shaped spectra, with signals in spectral regions typical of ring vibrations in large condensed aromatic carbon skeletons. Around 3000 cm^{-1}, the low-intense bands as a result of the stretching vibrations of aliphatic and aromatic C−H bonds were detected; in the medium-frequency range (between 1700 and 1000 cm^{-1}), a broad combination of peaks generated by the overlapping of carbon skeleton adsorption bands (C═O, C═C, C−C, and C−H−C−O stretching and bending modes) was found. A third group of bands characteristic of aromatic C−H out-of-plane (OPLA) bending modes was also detected between 1000 and 600 cm^{-1}.[27−31] With the increase in the pyrolysis temperature, the number of peaks in the infrared spectra is reduced; this is likely due to charring reactions and the removal of the labile functional groups (most likely oxygen-containing groups) that are favored at such high pyrolysis temperatures.[32]

For instance, the spectrum of sample CEL-530 is characterized by low-intense bands at 3016, 2988, and 2846 cm^{-1}, ascribed to aromatic and aliphatic C−H stretching modes in amorphous carbons.[28−31] The peak at 1695 cm^{-1} is associated with stretching modes of C═O moieties in conjugated systems, while the intense peak at 1575 cm^{-1} arises from C═C stretching modes in aromatic networks.[30,31] In the region between 900 and 1500 cm^{-1}, overlapped signals as a result of aromatic skeleton vibrations in carbon-defective networks (between 1100 and 1500 cm^{-1}), oxygen-containing groups (C−O−C glycosidic bonds around 1150 cm^{-1}), and C−H and C−OH ring deformations of carbohydratic moietes (1040 cm^{-1}) were detected.[32] In the 900−700 cm^{-1} region, three main peaks assigned to solo (870 cm^{-1}), duo (806 cm^{-1}), and trio (750 cm^{-1}) configurations (e.g., OPLA bending modes of aromatic C−H bonds)[28−31] were observed. The intensity of the three peaks is almost the same, indicating a high substitution degree in the aromatic network of this sample.[30,31]

The infrared spectrum of sample CEL-650 displayed features similar to CEL-530, with bands showing a less structured shape and an overall decrease in the intensity in most of them. In the case of sample CEL-700, the bands in the high-frequency region are almost not detectable and the peaks ascribable to C═O stretching modes and aromatic C−H OPLA disappeared. Only the peak at 1548 cm^{-1} as a result of C═C stretching modes and the overlapped peaks between 900 and 1500 cm^{-1} as a result of skeleton vibrations are still present.

Comparatively, the infrared spectra of the *P. nigra*-derived biochars were quite different compared to those of cellulose-derived materials. Indeed, in the region between 900 and 1700 cm^{-1}, peaks ascribable to the aromatic network of lignin are identified for PN-480 and PN-600. The spectra of the latter also featured low-intense bands as a result of aromatic and aliphatic C−H stretching in amorphous carbons (ca. 3045, 2925, and 2869 cm^{-1}). The bands associated with stretching modes of C═O in ketones or carboxylic moieties in conjugated systems (ca. 1700 cm^{-1}), C═C stretching modes in aromatic networks (ca. 1559 cm^{-1}), lignin-derived moieties (ca. 1444 and 1278 cm^{-1}), and C−OH stretching of pyranose rings from the holocellulosic fraction of *P. nigra* wood were also observed.[32]

In the region below 900 cm^{-1}, bending modes of solo, duo, and trio configurations with varied intensities were detected too; as opposed to the cellulose-derived biochars, the intensity of the solo signal was the highest, indicating a different but also high degree of condensation and substitution in the *P. nigra* wood-derived biochars. As for the impact of the pyrolysis temperature, samples PN-480 and PN-600 displayed similar spectral features, with a slight decrease in the intensity of the peak at 1590 cm^{-1}.

Textural Properties. It is well-known that chars usually display a constricted pore network comprised of nanopores of small dimensions accessible through pore mouths or necks of narrow dimensions.[33] As a result, gas adsorption at cryogenic temperatures (typically argon and nitrogen at −186 and −196 °C) may present kinetic restrictions and, thus, provide a limited value for the characterization of narrow micropores. Following International Union of Pure and Applied Chemistry (IUPAC) recommendations,[34] a combined approach based on the use of N_2 at −196 °C and CO_2 at 0 °C has been used to

DOI: 10.1021/acs.energyfuels.8b01058
Energy Fuels 2018, 32, 10218−10227

better describe the porosity of prepared biochars herein.[35] This allows for the detection of any kinetic limitations at cryogenic temperatures while enabling the evaluation of the narrow microporosity from the analysis of the CO_2 adsorption isotherms at 0 °C.

The N_2 adsorption/desorption isotherms at −196 °C of the prepared samples are shown in Figure 2. With the exception of PN-480, all of the biochars presented N_2 adsorption isotherms belonging to type I in the IUPAC classification,[34] characteristic of microporous materials. Also, all of the isotherms present a non-reversible desorption branch, which is indicative of materials displaying a constricted microporous structure, often reported for carbonaceous chars (as mentioned above).[33,35] This feature was less pronounced but still detected in the case of samples CEL-700 and CEL-650 (see magnification of the desorption branch in Figure S2 of the Supporting Information).

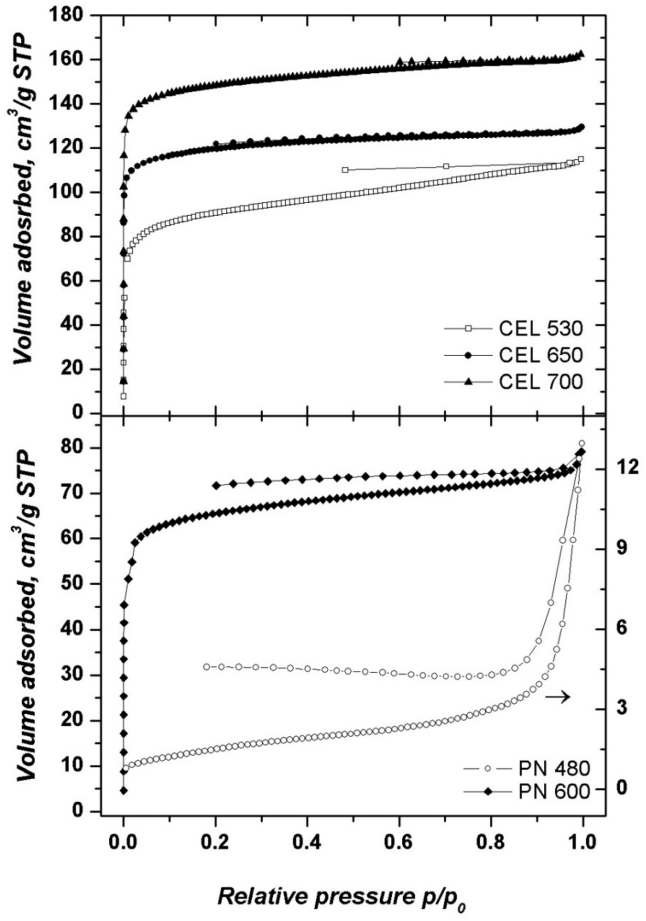

Figure 2. High-resolution N_2 adsorption/desorption isotherms at −196 °C of the synthesized biochars.

The nitrogen uptake is not very high for any of the obtained materials produced by steam-assisted slow pyrolysis, as expected for materials prepared upon carbonization at low temperature. Indeed, slow pyrolysis is typically carried out in an inert atmosphere, although the presence of oxidant agents, such as steam, has been reported to improve the porosity of the resulting chars as a result of the enhanced devolatilization favored by the efficient diffusion of steam in the precursor during pyrolysis, and, if the temperature is high enough, the capacity of steam to promote gasification reactions.[17−21] The temperatures selected herein for the steam-assisted slow pyrolysis tests were sufficiently low to limit the gasification of the feedstock, as evidenced in our previous work based on the analysis of the pyrolysis gas exhausts.[17,18,36−38] Thus, the porosity of the obtained chars is mainly due to the enhanced devolatilization of the raw precursor in the presence of steam.

The low nitrogen uptake is more pronounced in the case of PN-480; this feature can be attributed to either a poor textural development or the presence of a constricted pore structure, through which the diffusion of nitrogen at cryogenic temperatures is restricted.[39] To further discriminate this effect, the CO_2 adsorption isotherms at 0 °C were recorded (Figure 3) and analyzed using various methods. This allowed us to evaluate the so-called narrow microporosity (ultramicropores) of the biochars.[40] Data shown in Figure 3 and Table 2 confirmed that all of the samples displayed a well-developed narrow microporosity, including biochar PN-480. Interestingly, for all of the samples, the volume of total micropores (evaluated from N_2 data) is lower than the volume of narrow micropores evaluated from CO_2 data (Table 2); this confirmed the presence of nanopores of small dimensions in all of the biochars, which are not accessible to nitrogen as a result of diffusional limitations at −196 °C. Thus, sample PN-480 is a microporous biochar, despite the low BET surface area value.[40,41] The uptake of CO_2 at 0 °C increased with the pyrolysis temperature, indicating that the development of the narrow microporosity is favored at higher temperatures.

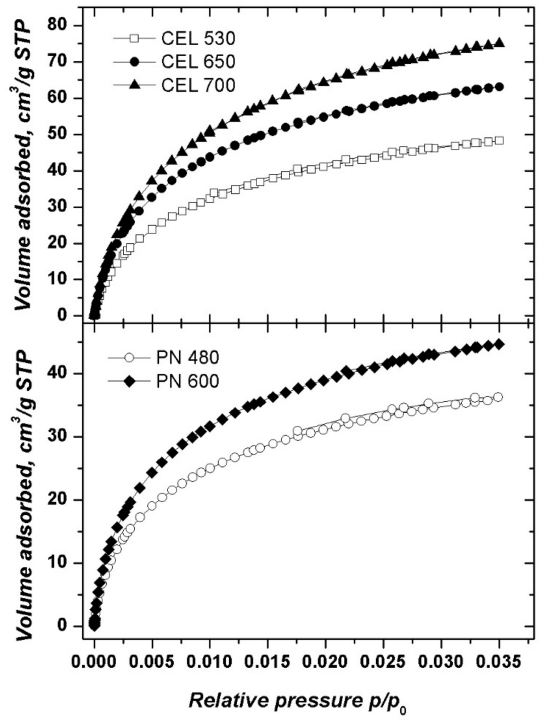

Figure 3. CO_2 adsorption/desorption isotherms at 0 °C of the synthesized biochars.

The average narrow micropore size (L) was estimated from the CO_2 adsorption isotherms at 0 °C using the empirical correlation proposed by Stoeckli−Ballerini,[42] valid for pore sizes between 0.35 and 1.3 nm.[43] As seen in Table 2, average values of ca. 0.6 and 0.55 nm were obtained for the cellulose- and *P. nigra*-derived biochars, respectively. These values are in

DOI: 10.1021/acs.energyfuels.8b01058
Energy Fuels 2018, 32, 10218−10227

Table 2. Main Textural Features of the Synthesized Biochars Obtained from the N_2 and CO_2 Adsorption/Desorption Isotherms at −196 and 0 °C, Respectively

	S_{BET} (m^2/g)	V_{total} [a] (cm^3/g)	$V_{micro}^{(DR,N_2)}$ [b] (cm^3/g)	$V_{micro}^{(DR,CO_2)}$ [c] (cm^3/g)	$V_{micro}^{(NLDFT,CO_2)}$ [d] (cm^3/g)	L [e] (nm)
CEL-530	351	0.177	0.141	0.160	0.138	0.61
CEL-650	473	0.199	0.183	0.220	0.169	0.60
CEL-700	593	0.250	0.220	0.250	0.205	0.60
PN-480	6	0.018	0.002	0.120	0.097	0.56
PN-600	217	0.121	0.093	0.140	0.129	0.54

[a]Total pore volume measured at $p/p_0 \sim 0.99$. [b]Total micropore volume evaluated by the DR method applied to N_2 adsorption data. [c]Narrow micropore volume evaluated by the DR method applied to CO_2 adsorption data. [d]Narrow micropore volume evaluated by NLDFT applied to CO_2 adsorption data. [e]Average narrow micropore size evaluated by the Stoeckli−Ballerini equation applied to CO_2 adsorption data.

line with the average micropore sizes reported for carbon-based materials with good CO_2 adsorption capacities.[44]

The BET surface area values ranged between 250 and 600 m^2/g, increasing as the pyrolysis temperature is raised (Table 2). The biochars synthesized from *P. nigra* wood presented lower surface area values than those from cellulose fibers, which may be attributed to the different composition of the biomass precursors. Indeed, *P. nigra* wood has two major components (e.g., lignin and hemicellulose) besides cellulose, which would prevent the development of an incipient porosity during the pyrolysis (likely the cellulose fraction is entrapped in a compact matrix).[36] On the other hand, the contribution of the ashes (Table 1) to the lower surface area should not be neglected, because this magnitude is expressed per gram of material.[37] To further evaluate this issue, biochar PN-600 was washed in a 1 M NaOH solution to remove the alkali-soluble inorganic species. The washed material displayed a negligible ash content, and despite the surface area and total pore volume increased by ca. 30% (Table S1 and Figure S3 of the Supporting Information), it still presented lower values than the biochars obtained from cellulose fibers.

CO_2 Uptake and Separation Capacity. The biochars showing the highest micropore volumes (namely, CEL-650, CEL-700, and PN-600) were selected for evaluating their ability to store and separate CO_2 at room temperature. The CO_2 isotherms at 25 °C for the selected samples are reported in Figure 4, along with the uptakes of N_2 and CH_4.

The highest CO_2 uptake was obtained for the cellulose-derived biochars (ca. 2.33 and 1.72 mmol/g for CEL-700 and CEL-650, respectively), with values almost twice as large as those of PN-600 (ca. 1.12 mmol/g). These values have been compared in Table 3 to the CO_2 uptakes of other biomass-derived carbon-based materials available in the literature. In Table 3, the CO_2 uptakes at 1, 0.15, and 0.3 atm were reported. The CO_2 uptakes at low pressures, namely, typical pressures for CO_2 capture in post-combustion purposes (0.15 atm) and biogas upgrading (0.30 atm), were included because, depending upon the pore size distribution, the fraction of the total CO_2 uptake at relatively low partial pressures could vary a lot for different carbon-based adsorbents.

Data in Table 3 provide evidence of a large variability of CO_2 uptake for biomass-derived carbons (covering biochars and biomass-derived activated carbons), likely as a result of the differences in the properties of the material associated with the nature of the starting feedstock and the synthesis conditions. Available data in the literature on CO_2 uptake of biochars are limited; however, it can be observed that the adsorption capacities of prepared biochars herein are comparable to those reported in the literature for other biomass-derived adsorbents obtained by slow pyrolysis or carbonization. For instance, the

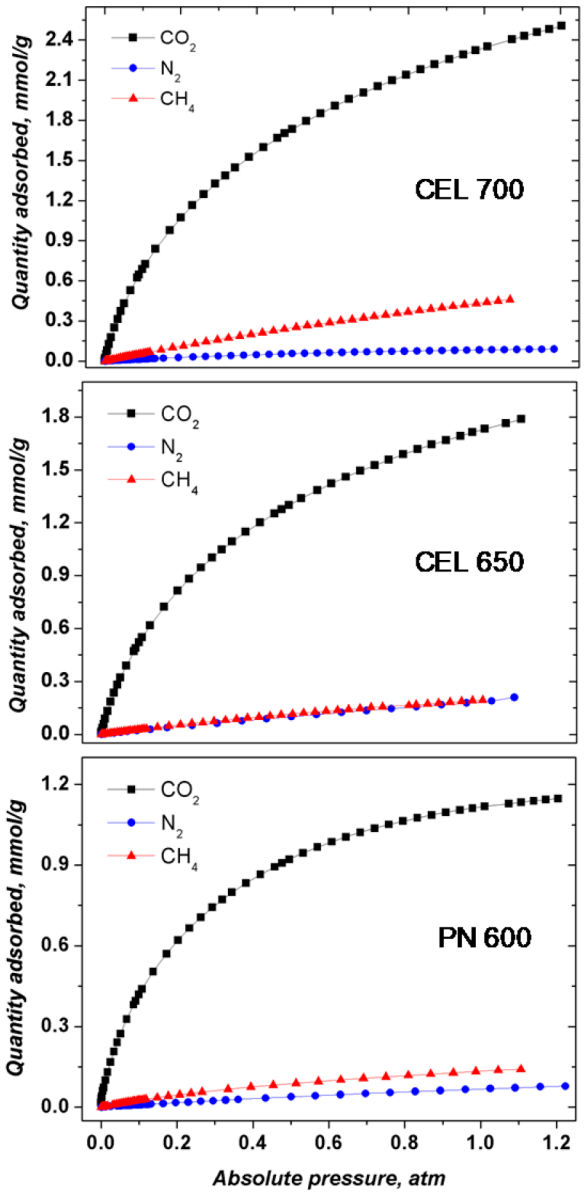

Figure 4. Equilibrium CO_2, N_2, and CH_4 uptakes at 25 °C of selected biochars.

CO_2 uptake of CEL-700 (2.33 mmol/g) is similar to that reported for cellulose fibers carbonized at 700 °C (2.2 mmol/g).[45] On the other hand, the adsorption capacities are lower than those of activated carbons prepared by physical and/or chemical activation of biomass. This is reasonable considering that the porosity of reported biochars herein is much lower

DOI: 10.1021/acs.energyfuels.8b01058
Energy Fuels 2018, 32, 10218−10227

Table 3. CO_2 Uptake at Room Temperature of the Synthesized Biochars[a]

feedstock	type	synthesis	S_{BET} (m^2/g)	V_{micro} (cm^3/g)	CO_2 uptake (mmol/g) 1 atm	0.15 atm	0.30 atm	reference
cellulose fibers	biochar	steam-assisted slow pyrolysis at 650 °C	473	0.183	1.72	0.7	1	this work
cellulose fibers	biochar	steam-assisted slow pyrolysis at 700 °C	593	0.220	2.33	0.9	1.4	this work
P. nigra wood	biochar	steam-assisted slow pyrolysis at 600 °C	217	0.093	1.12	0.5	0.75	this work
hickory wood	biochar	slow pyrolysis at 600 °C	401		1.39			46
sugar cane bagasse	biochar	slow pyrolysis at 600 °C	388		1.67			46
sawdust	biochar	gasification at 850 °C	182	0.0036	1.08			47
almond shell	biochar	single-step oxidation (3% O_2)	557	0.21[b]	2.11	~1.05	~1.5	48
olive stone	biochar	single-step oxidation (3% O_2)	697	0.27[b]	2.02	~0.8	~1.3	48
cellulose fibers	activated carbon	carbonization at 700 °C	499	0.193	2.21	~0.7	~1.2	45
cellulose fibers	activated carbon	carbonization at 700 °C and physical activation	599	0.229	2.61	~1	~1.6	45
cellulose fibers	activated carbon	carbonization at 800 °C and physical activation	863	0.334	3.78	~1.15	~2	45
pine nut shell	activated carbon	carbonization and chemical activation	1486	0.64	5.0	2	~2.9	44
olive stone	activated carbon	physical activation	1479	0.594	3.05	0.80	~1.4	49
lignin	activated carbon	chemical activation	2246	0.753	2.38	0.52	~0.9	49
lignin	activated carbon	carbonization	71	0.033	2.20	0.92	~1.4	49
eucalyptus wood	activated carbon	chemical activation	1889	1.063	2.98			50
bamboo	activated carbon	chemical activation	1846	0.36[b]	4.5	~1.2	~2.1	51
coconut shell	activated carbon	carbonization and physical activation	1327	0.55	3.9	~1.5	~1.9	52
African palm shells	activated carbon	carbonization	365	0.16	1.9	~0.9	~1.9	53
African palm shells	activated carbon	chemical activation	1250	0.55	4.4	~1.5	~1.9	53
vine shoots	activated carbon	physical activation	767	0.245	3.1	~1.2	~1.8	54
vine shoots	activated carbon	chemical activation	1439	0.493	4	~1.2	~2	54

[a]Data from selected best performing biomass-derived carbons reported in the literature are included for comparison purposes, along with selected characteristics and textural parameters (unless otherwise stated, micropore volumes were estimated from N_2 adsorption data and CO_2 uptakes were estimated at 25/30 °C and 1 bar). [b]Estimated from CO_2 adsorption data at 0 °C.

than that of activated carbons (steam-assisted slow pyrolysis conditions enhanced the surface area and overall microporosity of the prepared biochars).

It is well-known that the CO_2 adsorption capacity is strongly influenced by the adsorbent structural features and the operating conditions and that various mechanisms may be involved. In carbon-based adsorbents, the main parameters governing both the CO_2 uptake capacity and selectivity at low partial pressures and ambient temperature are the microporosity (volume and size) and functionalization of the pores.[16,49] At low pressure, the adsorption is favored in narrow micropores and the mechanism is based on short-range nonspecific interactions between the gas and adsorbent. At higher pressures, the surface coverage is the predominant mechanism and, therefore, wider micropores become more relevant (see ref 55 and references therein).

Considering this and aiming to better understand the CO_2 uptake of the prepared biochars under typical post-combustion conditions, we have evaluated the isosteric heat of CO_2 adsorption and discussed the adsorption capacity in terms of the physicochemical features of the biochars. The values of isosteric heat of CO_2 adsorption (determined using the Clausius−Clapeyron equation) were ca. 35, 22, and 34 kJ/mol for CEL-650, CEL-700, and PN-600, respectively (Figure S4 of the Supporting Information). The enthalpy values below 40 kJ/mol confirmed that physisorption is the dominant adsorption mechanism in these samples,[56] with the narrow micropores being the main adsorption sites. Indeed, the heat of adsorption of biochar CEL-700 was significantly lower than those of CEL-650 and PN-600, which is attributed to its wider distribution of micropores (Table 2). Additionally, the isosteric heats of adsorption were quite constant with the CO_2 coverage (Figure S3 of the Supporting Information), indicating energetically homogeneous adsorption sites. Overall, the CO_2 isosteric heats of adsorption are in line with those reported for other biochars obtained by slow pyrolysis.[46] These values are also within those recommended for post-combustion capture from an engineering point of view (between 30 and 60 kJ/mol).[55,56]

The ability of the biochars to adsorb N_2 and CH_4 at room temperature was also explored. As seen in Figure 3, the uptake of both gases is much lower than that of CO_2, indicating that the biochars are good materials for the separation of these gases. It is well-known that carbon adsorbents display a much lower affinity for nitrogen than carbon dioxide; in the case of methane, the lower uptake is attributed to the pore structure of the biochars, because methane is slightly bulkier than CO_2. CEL-700 exhibited the highest CH_4 uptake (ca. 0.44 mmol/g), and PN-600 exhibited the lowest CH_4 uptake (ca. 0.14 mmol/g). These values are within those reported for other biochars.[57]

As opposed to CO_2, where the uptake correlates with the volume of narrow micropores (Figure S5 of the Supporting Information), the uptake of CH_4 correlates well with the total micropore volume evaluated from the N_2 adsorption data (Figures S6 and S7 of the Supporting Information). This is due to the different sizes of the probe molecules and confirmed that materials with a narrow distribution of micropores are suitable for CO_2 storage and separation of CO_2/CH_4 mixtures. On the contrary, wider micropores would favor the uptake of methane,[55,58,59] as in the case of sample CEL-700.

Gas Selectivity (CO_2/N_2 and CO_2/CH_4). On the basis of their adsorption features and potential adequateness to

DOI: 10.1021/acs.energyfuels.8b01058
Energy Fuels 2018, 32, 10218−10227

separate CO_2 from N_2 and/or CH_4, we further investigated the selectivity of these biochars by the application of the IAST to the single-component experimental gas adsorption isotherms. IAST has been used for the prediction of multi-component adsorption mixtures on a wide range of porous materials having homogeneous energetic adsorption sites.[60,61] We have herein applied IAST to CO_2/N_2 and CO_2/CH_4 mixtures, representative of synthetic flue gases in post-combustion processes (with a v/v gas composition of 15:85) and natural gas upgrading processes (e.g., with v/v gas compositions of 30:70), respectively. The modeled isotherms are shown in Figure S8 of the Supporting Information, while IAST selectivities are compiled in Table 4. As seen, CEL-700 and PN-600 displayed higher CO_2/N_2 selectivities compared to CEL-650. However, a different trend was obtained for the separation of CO_2/CH_4, where biochar CEL-700 showed a lower selectivity value. This is in agreement with the wider micropore size distribution of this biochar (Table 2); thus, the micropores are accessible to methane. Furthermore, the CO_2/N_2 and CO_2/CH_4 selectivities show a good correlation with textural parameters of the biochars in terms of the pore volume and average micropore size, respectively (Figure S9 of the Supporting Information).

Table 4 also compiles CO_2/N_2 selectivity values reported in the literature for other adsorbents evaluated for typical post-combustion flue gas mixtures (i.e., CO_2/N_2, 15:85, v/v). The selectivities of our biochars are within the range of those reported for some activated carbons with much higher porosity but lower than those of synthetic polymers, zeolites and metal−organic framework (MOF). It is worth noting that only few data are available about ideal CO_2/CH_4 selectivities for a typical natural gas upgrading (CO_2/CH_4, 30:70, v/v); therefore, it appears that the selectivities of the biochars, object of this work, are quite higher than those reported for synthetic carbons (Table 4).

Table 4. CO_2/N_2 and CO_2/CH_4 Selectivities at 25 °C Calculated from IAST Simulations for Different Gas Mixtures ($S_{ij} = C_i/x_j/C_j/x_i$)[a]

adsorbent type	CO_2/N_2 (15:85)	CO_2/CH_4 (30:70)	reference
cellulose fibers biochar (CEL-650)	34 (6)	32 (13.7)	this work
cellulose fibers biochar (CEL-700)	119 (21)	14 (6)	this work
P. nigra wood biochar (PN-600)	105 (18.6)	34 (14.7)	this work
synthetic carbon (C125-220)	(4.0)[b]	7.2[b]	61
synthetic carbon (C200-180)	(3.9)[b]	2.1[b]	61
synthetic carbon (C_{ReHy12}@600)	(7.1)[b]		62
synthetic carbon (C_{ReHy12}@700)	(5.3)[b]		62
synthetic carbon (C_{ReHy13}@450)	(9.4)[b]		62
synthetic carbon (C_{ReHy13}@500)	(13.0)[b]		62
N-doped carbon (IBN9-NC1)	~32		63
N-doped carbon (IBN9-NC1-A)	~24		63
activated carbon (pomegranate peels)	15.1		64
activated carbon (carrot peels)	8.1		64
activated carbon (fern leaves)	5.6		64
activated carbon (mistletoe branches)	11.4		64
activated carbon (mistletoe leaves)	12.0		64
activated carbon (kiwi fruit peels)	10.6		64
activated carbon (sugar beet pulp)	2.8		64
synthetic carbons (CKHP800-2)	50		65
sulfonate-grafted porous polymer (PPN-6-SO_3H)	155[c]		66
sulfonate-grafted porous polymer (PPN-6-SO_3Li)	414[c]		66
zeolite NaX	110[c]		66
MOF-505	7.6		67
composite MOF-505@5GO	8.6		67
UiO-66	19.4		68
UiO-66(Zr)−$(COOH)_2$	37.9		68
UiO-66(Zr)−$(COOLi)_2$	50.8		68
UiO-66(Zr)−$(COONa)_2$	58.0		68
UiO-66(Zr)−$(COOK)_2$	69.3		68
MIL-101 (Cr)	21		69
MIL-101 (Cr, Mg)	86		69

[a]Data of carbon materials available in the literature are also compiled for comparison; selectivity values in parentheses have been calculated as $S_{ij} = C_i/C_j$. Unless otherwise stated, experimental conditions were similar for all of the samples. [b]Values calculated at 1.2 bar. [c]Values calculated at 22 °C.

CONCLUSION

The ability of biochars produced by slow steam-assisted pyrolysis to store and separate CO_2 at room temperature was investigated, and some correlations with the biochar textural properties were highlighted. Predictions of the adsorption of binary gaseous mixtures (CO_2/CH_4 and CO_2/N_2) by applying the IAST were also carried out. Moreover, the storage and selectivity properties of selected samples have been compared to available literature data (available data in the literature on CO_2 uptake of biochars is limited).

The collected data revealed that the adsorption capacities (1.5−2.5 mmol/g of CO_2 uptake range) of selected biochars (from cellulose fibers and *P. nigra* wood) were comparable to those reported in the literature for other biomass-derived adsorbents obtained by slow pyrolysis or carbonization but lower than those of activated carbons prepared by physical and/or chemical activation of biomass. The suitability of the selected biochars for CO_2 uptake was also proven by the good correlation obtained between the amount of CO_2 adsorbed and the pore volumes (biochars exhibited a narrow microporosity, whose volume increases with the increasing of the pyrolysis temperature and average pore diameters between 0.55 and 0.6 nm). The samples also exhibited quite good selectivities for CO_2 over both N_2 and CH_4 [between 34 and 119 for a CO_2/N_2 mixture in typical post-combustion conditions (15:85, v/v) and between 14 and 34 for a CO_2/CH_4 mixture typical of natural gas upgrading (30:70, v/v)]. In particular, the CO_2/N_2 selectivity values resulted within the range of those reported for some activated carbons with much higher porosity but lower than those of synthetic polymers, such as zeolites and MOFs.

Overall, the results reported in this work demonstrate that using the biochar as an adsorbent in the gas treatment process could be a sustainable approach and this is even truer when biochar production represents a route for the valorization of a waste material.

ASSOCIATED CONTENT

Supporting Information

The Supporting Information is available free of charge on the ACS Publications website at DOI: 10.1021/acs.energyfuels.8b01058.

DOI: 10.1021/acs.energyfuels.8b01058
Energy Fuels 2018, 32, 10218−10227

Thermogravimetry profiles of biochar precursors (Figure S1), N_2 isotherms of cellulose-derived biochar (Figure S2), N_2 and CO_2 isotherms of PN-600 NaOH (Figure S3), main textural features of samples PN-600 and PN-600 NaOH (Table S1), isosteric heats of adsorption (Figure S4), correlation graphics (Figures S5−S7 and S9), and IAST-modeled curves (Figure S8) (PDF)

AUTHOR INFORMATION

Corresponding Author

*Telephone: +39-0817682230. E-mail: gargiulo@irc.cnr.it.

ORCID

Valentina Gargiulo: 0000-0002-6517-2263
Paola Giudicianni: 0000-0002-6700-8205
Michela Alfè: 0000-0001-8930-1210

Notes

The authors declare no competing financial interest.

ACKNOWLEDGMENTS

This paper stems from the cooperation between the authors in the framework of the COST Action SMARTCATs (CM1404, www.smartcats.eu), supported by COST (European Cooperation in Science and Technology, www.cost.eu). Valentina Gargiulo acknowledges the support of the Short Term Scientific Mission Program of SMARTCATs for her stay at CEMTHI, CNRS (Orléans, France). Conchi O. Ania and Alicia Gomis-Berenguer thank the financial support of the ERC Consolidator Grant (648161, PHOROSOL). A large part of the experimental work was made possible thanks to the financial support of the Piano Annuale della Ricerca MiSE-CNR under the projects "Sistemi Elettrochimici per l'Accumulo di Energia" and "Microbio-CHP".

REFERENCES

(1) Cha, J. S.; Park, S. H.; Jung, S.-C.; Ryu, C.; Jeon, J.-K.; Shin, M.-C.; Park, Y.-K. Production and utilization of biochar: A review. *J. Ind. Eng. Chem.* **2016**, *40*, 1−15.

(2) Kan, T.; Strezov, V.; Evans, T. J. Lignocellulosic biomass pyrolysis: A review of product properties and effects of pyrolysis parameters. *Renewable Sustainable Energy Rev.* **2016**, *57*, 1126−1140.

(3) Xu, R.; Ferrante, L.; Hall, K.; Briens, C.; Berruti, F. Thermal self-sustainability of biochar production by pyrolysis. *J. Anal. Appl. Pyrolysis* **2011**, *91*, 55−66.

(4) Ahmad, M.; Rajapaksha, A. U.; Lim, J. E.; Zhang, M.; Bolan, N.; Mohan, D.; Vithanage, M.; Lee, S. S.; Ok, Y. S. Biochar as a sorbent for contaminant management in soil and water: A review. *Chemosphere* **2014**, *99*, 19−33.

(5) Lehmann, J.; Gaunt, J.; Rondon, M. Bio-char sequestration in terrestrial ecosystems—A review. *Mitig. Adapt. Strat. Gl.* **2006**, *11*, 403−427.

(6) Qambrani, N. A.; Rahman, M. M.; Won, S.; Shim, S.; Ra, C. Biochar properties and eco-friendly applications for climate change mitigation, waste management, and wastewater treatment: A review. *Renewable Sustainable Energy Rev.* **2017**, *79*, 255−273.

(7) Matovic, D. Biochar as a viable carbon sequestration option: Global and Canadian perspective. *Energy* **2011**, *36*, 2011−2016.

(8) Chen, Y.; Zhang, X.; Chen, W.; Yang, H.; Chen, H. The structure evolution of biochar from biomass pyrolysis and its correlation with gas pollutant adsorption performance. *Bioresour. Technol.* **2017**, *246*, 101−109.

(9) Oliveira, F. R.; Patel, A. K.; Jaisi, D. P.; Adhikari, S.; Lu, H.; Khanal, S. K. Environmental application of biochar: Current status and perspectives. *Bioresour. Technol.* **2017**, *246*, 110−122.

(10) Moreira, M. T.; Noya, I.; Feijoo, G. The prospective use of biochar as adsorption matrix—A review from a lifecycle perspective. *Bioresour. Technol.* **2017**, *246*, 135−141.

(11) Bamdad, H.; Hawboldt, K.; MacQuarrie, S. A review on common adsorbents for acid gases removal: Focus on biochar. *Renewable Sustainable Energy Rev.* **2018**, *81*, 1705−1720.

(12) Tan, X.-f.; Liu, S.-b.; Liu, Y.-g.; Gu, Y.-l.; Zeng, G.-m.; Hu, X.-j.; Wang, X.; Liu, S.-h.; Jiang, L.-h. Biochar as potential sustainable precursors for activated carbon production: Multiple applications in environmental protection and energy storage. *Bioresour. Technol.* **2017**, *227*, 359−372.

(13) Dobele, G.; Dizhbite, T.; Gil, M. V.; Volperts, A.; Centeno, T. A. Production of nanoporous carbons from wood processing wastes and their use in supercapacitors and CO_2 capture. *Biomass Bioenergy* **2012**, *46*, 145−154.

(14) Nanda, S.; Reddy, S. N.; Mitra, S. K.; Kozinski, J. A. The progressive routes for carbon capture and sequestration. *Energy Sci. Eng.* **2016**, *4* (2), 99−122.

(15) D'Alessandro, D. M.; Smit, B.; Long, J. R. Carbon dioxide capture: Prospects for new materials. *Angew. Chem., Int. Ed.* **2010**, *49*, 6058−6082.

(16) Martin, C. F.; Plaza, M. G.; Pis, J. J.; Rubiera, F.; Pevida, C.; Centeno, T. A. On the limits of CO2 capture capacity of carbons. *Sep. Purif. Technol.* **2010**, *74*, 225−229.

(17) Giudicianni, P.; Pindozzi, S.; Grottola, C. M.; Stanzione, F.; Faugno, S.; Fagnano, M.; Fiorentino, N.; Ragucci, R. Pyrolysis for exploitation of biomasses selected for soil phytoremediation: Characterization of gaseous and solid products. *Waste Manage.* **2017**, *61*, 288−299.

(18) Ragucci, R.; Giudicianni, P.; Cavaliere, A. Cellulose slow pyrolysis products in a pressurized steam flow reactor. *Fuel* **2013**, *107*, 122−130.

(19) Cyganiuk, A.; Gorska, O.; Olejniczak, A.; Lukaszewicz, J. P. Pyrolitic production of microporous charcoals from different wood resources. *J. Anal. Appl. Pyrolysis* **2012**, *98*, 15−21.

(20) Minkova, V.; Razvigorova, M.; Bjornbom, E.; Zanzi, R.; Budinova, T.; Petrov, N. Effect of water vapour and biomass nature on the yield and quality of the pyrolysis products from biomass. *Fuel Process. Technol.* **2001**, *70*, 53−61.

(21) Khezami, L.; Chetouani, A.; Taouk, B.; Capart, R. Production and characterisation of activated carbon from wood components in powder: Cellulose, lignin, xylan. *Powder Technol.* **2005**, *157*, 48−56.

(22) Andrade, M.; Parra, J. B.; Haro, M.; Mestre, A. S.; Carvalho, A. P.; Ania, C. O. Characterization of the different fractions obtained from the pyrolysis of rope industry waste. *J. Anal. Appl. Pyrolysis* **2012**, *95*, 31−37.

(23) Jagiello, J.; Ania, C. O.; Parra, J. B.; Cook, C. Dual Gas Analysis of Microporous Carbons Using 2D-NLDFT Heterogeneous Surface Model and Combined Adsorption Data of N_2 And CO_2. *Carbon* **2015**, *91*, 330−337.

(24) Myers, A. L.; Prausnitz, J. M. Thermodynamics of mixed-gas adsorption. *AIChE J.* **1965**, *11*, 121−127.

(25) Jensen, A. L. C. R. C.; Seaton, N. A. An Isotherm Equation for Adsorption to High Pressures in Microporous Adsorbents. *Langmuir* **1996**, *12*, 2866−2867.

(26) Suliman, W.; Harsh, J. B.; Abu-Lail, N. I.; Fortuna, A.-M.; Dallmeyer, I.; Garcia-Perez, M. Influence of feedstock source and pyrolysis temperature on biochar bulk and surface properties. *Biomass Bioenergy* **2016**, *84*, 37−48.

(27) Silverstein, R. M.; Webster, F. X.; Kiemle, D. J. *Spectrometric Identification of Organic Compounds*, 4th ed.; Wiley: Hoboken, NJ, 2008.

(28) Galvez, A.; Herlin-Boime, N.; Reynaud, C.; Clinard, C.; Rouzaud, J.-N. Carbon nanoparticles from laser pyrolysis. *Carbon* **2002**, *40*, 2775−2789.

(29) Centrone, A.; Brambilla, L.; Renouard, T.; Gherghel, L.; Mathis, C.; Müllen, K.; Zerbi, G. Structure of new carbonaceous material. The role of vibrational spectroscopy. *Carbon* **2005**, *43*, 1593−1609.

DOI: 10.1021/acs.energyfuels.8b01058
Energy Fuels 2018, 32, 10218−10227

(30) Gargiulo, V.; Apicella, B.; Alfè, M.; Russo, C.; Stanzione, F.; Tregrossi, A.; Amoresano, A.; Millan, M.; Ciajolo, A. Structural Characterization of Large Polycyclic Aromatic Hydrocarbons. Part 1: The Case of Coal Tar Pitch and Naphthalene-Derived Pitch. *Energy Fuels* **2015**, *29*, 5714−5722.
(31) Gargiulo, V.; Apicella, B.; Stanzione, F.; Tregrossi, A.; Millan, M.; Ciajolo, A.; Russo, C. Structural Characterization of Large Polycyclic Aromatic Hydrocarbons. Part 2: Solvent-Separated Fractions of Coal Tar Pitch and Naphthalene-Derived Pitch. *Energy Fuels* **2016**, *30*, 2574−2583.
(32) Keiluweit, M.; Nico, P. S.; Johnson, M. G.; Kleber, M. Dynamic Molecular Structure of Plant Biomass-Derived Black Carbon (Biochar). *Environ. Sci. Technol.* **2010**, *44*, 1247−1253.
(33) Marsh, H.; Rodriguez-Reinoso, F. *Activated Carbon*; Elsevier Science & Technology Books: Amsterdam, Netherlands, Aug 2006; ISBN: 0080444636, DOI: 10.1016/B978-0-08-044463-5.X5013-4.
(34) Thommes, M.; Kaneko, K.; Neimark, A. V.; Olivier, J. P.; Rodriguez-Reinoso, F.; Rouquerol, J.; Sing, K. S. W. Physisorption of gases, with special reference to the evaluation of surface area and pore size distribution (IUPAC Technical Report). *Pure Appl. Chem.* **2015**, *87*, 1051−1069.
(35) Rouquerol, F.; Rouquerol, J.; Sing, K. S. W.; Llewellyn, P.; Maurin, G. *Adsorption by Powders and Porous Solids Principles, Methodology and Applications*, 2nd ed.; Elsevier Science & Technology Books: Amsterdam, Netherlands, 2014; ISBN: 978-0-08-097035-6, DOI: 10.1016/C2010-0-66232-8.
(36) Giudicianni, P.; Cardone, G.; Ragucci, R. Cellulose, hemicellulose and lignin slow steam pyrolysis: Thermal decomposition of biomass components mixtures. *J. Anal. Appl. Pyrolysis* **2013**, *100*, 213−222.
(37) Giudicianni, P.; Cardone, G.; Sorrentino, G.; Ragucci, R. Hemicellulose, cellulose and lignin interactions on Arundo donax steam assisted pyrolysis. *J. Anal. Appl. Pyrolysis* **2014**, *110*, 138−146.
(38) Gargiulo, V.; Giudicianni, P.; Alfè, M.; Ragucci, R. Influence of possible interactions between biomass organic components and alkali metal ions on steam assisted pyrolysis: A case study on *Arundo donax*. *J. Anal. Appl. Pyrolysis* **2015**, *112*, 244−252.
(39) Lozano-Castello, D.; Cazorla-Amoros, D.; Linares-Solano, A. Usefulness of CO_2 adsorption at 273 K for the characterization of porous carbons. *Carbon* **2004**, *42*, 1233−1242.
(40) Garrido, J.; Linares-Solano, A.; Martin-Martinez, J. M.; Molina-Sabio, M.; Rodriguez-Reinoso, F.; Torregrosa, R. Use of nitrogen vs. carbon dioxide in the characterization of activated carbons. *Langmuir* **1987**, *3*, 76−81.
(41) Silvestre-Albero, J.; Silvestre-Albero, A.; Rodriguez-Reinoso, F.; Thommes, M. Physical characterization of activated carbons with narrow microporosity by nitrogen (77.4 K), carbon dioxide (273 K) and argon (87.3 K) adsorption in combination with immersion calorimetry. *Carbon* **2012**, *50*, 3128−3133.
(42) Stoeckli, F.; Ballerini, L. Evolution of microporosity during activation of carbon. *Fuel* **1991**, *70* (4), 557−559.
(43) Cazorla-Amorós, D.; Alcañiz-Monge; de la Casa-Lillo, M. A.; Linares-Solano, A. CO_2 As an Adsorptive To Characterize Carbon Molecular Sieves and Activated Carbons. *Langmuir* **1998**, *14*, 4589−4596.
(44) Deng, S.; Wei, H.; Chen, T.; Wang, B.; Huang, J.; Yu, G. Superior CO_2 adsorption on pine nut shell-derived activated carbons and the effective micropores at different temperatures. *Chem. Eng. J.* **2014**, *253*, 46−54.
(45) Heo, Y.-J.; Park, S.-J. A role of steam activation on CO_2 capture and separation of narrow microporous carbons produced from cellulose fibers. *Energy* **2015**, *91*, 142−150.
(46) Creamer, A. E.; Gao, B.; Zhang, M. Carbon dioxide capture using biochar produced from sugarcane bagasse and hickory wood. *Chem. Eng. J.* **2014**, *249*, 174−179.
(47) Madzaki, H.; Ghani, W. A. W.; AB, K.; Rebitanim, N. Z.; Alias, A. B. Carbon Dioxide Adsorption on Sawdust Biochar. *Procedia Eng.* **2016**, *148*, 718−725.
(48) Plaza, M. G.; González, A. S.; Pis, J. J.; Rubiera, F.; Pevida, C. Production of microporous biochars by single-step oxidation: Effect of activation conditions on CO_2 capture. *Appl. Energy* **2014**, *114*, 551−562.
(49) Calvo-Muñoz, E. M.; García-Mateos, F. J.; Rosas, J. M.; Rodríguez-Mirasol, J.; Cordero, T. Biomass Waste carbon Materials as adsorbents for CO_2 capture under post-combustion conditions. *Front. Mater.* **2016**, *3*, 23.
(50) Heidari, A.; Younesi, H.; Rashidi, A.; Ghoreyshi, A. A. Adsorptive removal of CO_2 on highly microporous activated carbons prepared from *Eucalyptus camaldulensis* wood: Effect of chemical activation. *Chem. Eng. J.* **2014**, *254*, 503−513.
(51) Wei, H.; Deng, S.; Hu, B.; Chen, Z.; Wang, B.; Huang, J.; Yu, G. Granular Bamboo-Derived Activated Carbon for High CO_2 Adsorption: The Dominant Role of Narrow Micropores. *ChemSusChem* **2012**, *5*, 2354−2360.
(52) Ello, A. S.; de Souza, L. K. C.; Trokourey, A.; Jaroniec, M. Coconut shell-based microporous carbons for CO_2 capture. *Microporous Mesoporous Mater.* **2013**, *180*, 280−283.
(53) Ello, A. S.; de Souza, L. K. C.; Trokourey, A.; Jaroniec, M. Development of microporous carbons for CO_2 capture by KOH activation of African palm shells. *J. CO_2 Util.* **2013**, *2*, 35−38.
(54) Manyà, J. J.; González, B.; Azuara, M.; Arner, G. Ultra-Microporous Adsorbents Prepared from Vine Shoots-Derived Biochar with High CO_2 Uptake and CO_2/N_2 Selectivity. *Chem. Eng. J.* **2018**, *345*, 631−639.
(55) Álvarez-Gutiérrez, N.; Gil, M. V.; Rubiera, F.; Pevida, C. Adsorption performance indicators for the CO_2/CH_4 separation: Application to biomass-based activated carbons. *Fuel Process. Technol.* **2016**, *142*, 361−369.
(56) Samanta, A.; Zhao, A.; Shimizu, G. K. H.; Sarkar, P.; Gupta, R. Post-Combustion CO_2 Capture Using Solid Sorbents: A Review. *Ind. Eng. Chem. Res.* **2012**, *51*, 1438−1463.
(57) Sadasivam, B. Y.; Reddy, K. R. Adsorption and transport of methane in biochars derived from waste wood. *Waste Manage.* **2015**, *43*, 218−229.
(58) Kumar, K. V.; Preuss, K.; Titirici, M.-M.; Rodríguez-Reinoso, F. Nanoporous Materials for the Onboard Storage of Natural Gas. *Chem. Rev.* **2017**, *117*, 1796−1825.
(59) Rodríguez-Reinoso, F.; Almansa, C.; Molina-Sabio, M. Contribution to the evaluation of density of methane adsorbed on activated carbon. *J. Phys. Chem. B* **2005**, *109*, 20227−20231.
(60) Gutierrez, M. C.; Carriazo, D.; Ania, C. O.; Parra, J. B.; Ferrer, M. L.; del Monte, F. Deep eutectic solvents as both precursors and structure directing agents in the synthesis of nitrogen doped hierarchical carbons highly suitable for CO_2 capture. *Energy Environ. Sci.* **2011**, *4*, 3535−3544.
(61) Patiño, J.; Gutiérrez, M. C.; Carriazo, D.; Ania, C. O.; Parra, J. B.; Ferrer, M. L.; del Monte, F. Deep eutectic assisted synthesis of carbon adsorbents highly suitable for low-pressure separation of CO_2-CH_4 gas mixtures. *Energy Environ. Sci.* **2012**, *5*, 8699−8707.
(62) Patiño, J.; Gutiérrez, M. C.; Carriazo, D.; Ania, C. O.; Fierro, J. L. G.; Ferrer, M. L.; del Monte, F. DES assisted synthesis of hierarchical nitrogen-doped carbon molecular sieves for selective CO_2 versus N_2 adsorption. *J. Mater. Chem. A* **2014**, *2*, 8719−8729.
(63) Zhao, Y.; Zhao, L.; Yao, K. X.; Yang, Y.; Zhang, Q.; Han, Y. Novel porous carbon materials with ultrahigh nitrogen contents for selective CO_2 capture. *J. Mater. Chem.* **2012**, *22*, 19726−19731.
(64) Serafin, J.; Narkiewicz, U.; Morawski, A. W.; Wróbel, R. J.; Michalkiewicz, B. Highly microporous activated carbons from biomass for CO_2 capture and effective micropores at different conditions. *J. CO_2 Util.* **2017**, *18*, 73−79.
(65) Adeniran, B.; Masika, E.; Mokaya, R. A family of microporous carbons prepared via a simple metal salt carbonization route with high selectivity for exceptional gravimetric and volumetric post-combustion CO_2 capture. *J. Mater. Chem. A* **2014**, *2*, 14696−14710.
(66) Lu, W.; Yuan, D.; Sculley, J.; Zhao, D.; Krishna, R.; Zhou, H. C. Sulfonate-Grafted Porous Polymer Networks for Preferential CO_2

DOI: 10.1021/acs.energyfuels.8b01058
Energy Fuels 2018, 32, 10218−10227

Adsorption at Low Pressure. *J. Am. Chem. Soc.* **2011**, *133*, 18126−18129.
(67) Chen, Y.; Lv, D.; Wu, J.; Xiao, J.; Xi, H.; Xia, Q.; Li, Z. A new MOF-505@GO composite with high selectivity for CO_2/CH_4 and CO_2/N_2 separation. *Chem. Eng. J.* **2017**, *308*, 1065−1072.
(68) Hu, Z.; Khurana, M.; Seah, Y. H.; Zhang, M.; Guo, Z.; Zhao, D. Ionized Zr-MOFs for highly efficient post-combustion CO_2 capture. *Chem. Eng. Sci.* **2015**, *124*, 61−69.
(69) Zhou, Z.; Mei, L.; Ma, C.; Xu, F.; Xiao, J.; Xia, Q.; Li, Z. A novel bimetallic MIL-101(Cr, Mg) with high CO_2 adsorption capacity and CO_2/N_2 selectivity. *Chem. Eng. Sci.* **2016**, *147*, 109−117.

DOI: 10.1021/acs.energyfuels.8b01058
Energy Fuels 2018, 32, 10218−10227